Journal of Alloys and Compounds 525 (2012) 120–125

Contents lists available at SciVerse ScienceDirect

Journal of Alloys and Compounds

journal homepage: www.elsevier.com/locate/jallcom

Low temperature fired and electromagnetic properties of a novel ferroelectric/ferromagnetic composite material

Weiwei Ling[a,*], Hai Nie[a], Yuanxun Li[b], Huaiwu Zhang[b]

[a] Department of Communication Engineering, Chengdu University of Information Technology, Chengdu 610225, People's Republic of China
[b] State Key Laboratory of Electronic Thin Films and Integrated Devices, University of Electronic Science and Technology of China, Chengdu 610054, People's Republic of China

ARTICLE INFO

Article history:
Received 25 September 2011
Received in revised form 27 January 2012
Accepted 5 February 2012
Available online xxx

Keywords:
Ferroelectric–ferromagnetic composites
LTCC
Magnetic properties
Dielectric properties
Maxwell Garnett mixing rule

ABSTRACT

A series of $Bi_4Ti_3O_{12}/Ni_{0.25}Cu_{0.2}Zn_{0.55}Fe_2O_4$ ferroelectric–ferromagnetic composites were prepared by the usual ceramic technology and sintered at 900 °C to adapt to the low temperature cofired ceramic (LTCC) technology. Among all samples, the relative density changes in the range of 94.9–96.4% and reaches the highest value in the composite with 30 wt% $Bi_4Ti_3O_{12}$ (BIT). When BIT content increases from 0 to 90 wt%, the magnetic and dielectric properties show different change trends: the permeability (real part) at 1 MHz reaches the maximum 170 in the composite with 10 wt% BIT at first, and then gradually decreases from 170 to 1.4, while the saturation magnetization decrease from 2.85×10^5 A/m to 1.6×10^4 A/m; the dielectric loss tangent obtains a maximum value about 0.47 in the composite with 10 wt% BIT at first, and then decreases sharply, while the permittivity (real part) at 1 MHz increases from 8.8 to 100.3. The Maxwell Garnett mixing rule was used to predict the magnetic and dielectric properties of the composites with different assumptions. The calculated results basing on BIT matrix were more approximate to the measured in comparison to that basing on ferrite matrix.

1. Introduction

With the development of electronic technology, more and more attentions have been paid to the ferroelectric–ferromagnetic composite materials for fabricating microwave devices, electromagnetic interference (EMI) filters, miniature antennas, etc. [1–12]. There are many researches focus on combining Ni–Zn or Ni–Cu–Zn ferrites with different ferroelectric materials such as $BaTiO_3$ [3–7], $Ba_xSr_{(1-x)}TiO_3$ [8], $Pb(Mg_{1/3}Nb_{2/3})O_3$–$Pb(Zn_{1/3}Nb_{2/3})O_3$–$PbTiO_3$ (PMZNT) [9], $0.8Pb(Ni_{1/3}Nb_{2/3})O_3$–$0.2PbTiO_3$ (PNNT) [10], $Pb(Ni_{1/3}Nb_{2/3})O_3$–$PbZrO_3$–$PbTiO_3$ (PNZT) [11], and various composite materials showing simultaneous ferroelectric and ferromagnetic characteristics have been successfully prepared. Meanwhile, to meet the requirements of miniaturization and excellent high frequency performance of the electronic devices, the ceramic materials that can adapt to the high level of passive integration are needed. This trend facilitates popularization of low temperature cofired ceramic (LTCC) technology in production. Hence, developing the ceramic composite materials which can be cofired with low-melting internal electrodes, such as Ag [13], is also required. Some methods including addition of low-melting oxides or glasses [5–7,14] and using low-melting ceramic as a component of the composite [9–11] have been employed to decrease the sintering temperature. In our previous works, we aim to realize the low temperature sintering of the $BaTiO_3$/Ni–Cu–Zn ferrite composites with different fluxing agents [6,7]. However, existing as impurities, fluxing agents result in the deterioration of the magnetic and dielectric properties of the composites, and furthermore, the volatile components in the fluxing agents may weaken the adhesive force between internal electrode materials and the ceramic composites.

Considering the above factors, we endeavor to look for an appropriate low-melting ferroelectric material instead of high-melting $BaTiO_3$. Ferroelectric $Bi_4Ti_3O_{12}$ ceramic has high dielectric constant, high Curie temperature and low melting point, and can be applied in liquid phase sintering [15,16]. Its improvement effects on the sintered process and magnetic property of Ni–Cu–Zn ferrites have been proved by our previous experiments [17]. In this work, the sintered temperature of each $Bi_4Ti_3O_{12}$/Ni–Cu–Zn ferrite composite is fixed at 900 °C in order to meet the requirement of cofiring with Ag. The influence of different compositions on the microstructures, magnetic and dielectric properties of the composites has been investigated.

2. Experimental procedure

The analytical grade NiO, CuO, ZnO and Fe_2O_3 were weighted following the formula $Ni_{0.25}Cu_{0.2}Zn_{0.55}Fe_2O_4$ (NCZF). These basic oxides were mixed and wet-milled for 12 h and pre-sintered at 800 °C for 2 h. The $Bi_4Ti_3O_{12}$ (BIT) was prepared through solid-state reaction using analytical grade Bi_2O_3 and TiO_2 and pre-sintered at 770 °C.

* Corresponding author. Tel.: +86 28 85966249.
E-mail address: lingweiwei@163.com (W. Ling).

0925-8388/$ – see front matter © 2012 Elsevier B.V. All rights reserved.
doi:10.1016/j.jallcom.2012.02.044

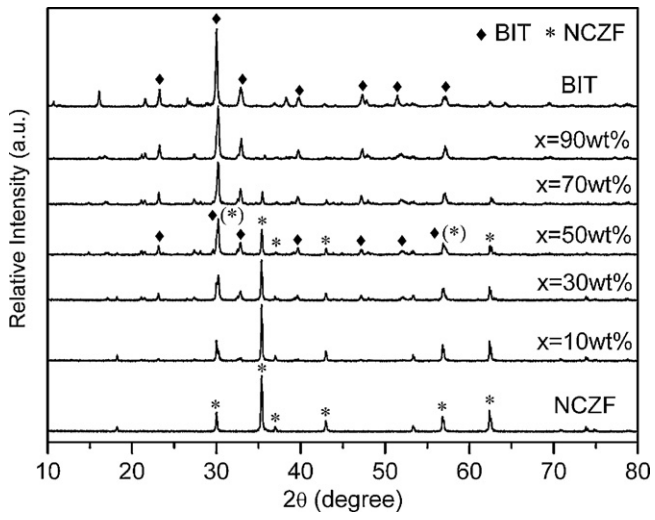

Fig. 1. X-ray diffraction patterns for the samples sintered at 900 °C.

The above two pre-sintered powders were mixed at various compositions of $(1-x)$ NCZF + x BIT (x = 0–100 wt%), and then wet-milled for 12 h. The mixtures were dried, mixed with 10 wt% poly(ethylene glycol) binder, sieved through 0.15 mm mesh and pressed at 5 MPa to the shape of toroids (Ø 18 mm × 8 mm) and pellets (Ø 18 mm) with 2–3 mm thickness. In these toroids and pellets, the ones with x = 10 wt%, 30 wt%, 50 wt%, 70 wt%, and 90 wt% were sintered at 900 °C in air for 3 h to yield the composite samples, the others with x = 0 wt% (NCZF) and 100 wt% (BIT) were sintered in ranges of 900–1100 °C and 850–950 °C, respectively.

The phase structures of the samples were investigated by X-ray diffractometer (XRD, RINT2000, Rigaku Co.) with Cu Kα radiation. The microstructures on the cross section of the samples were examined by scanning electron microscope (SEM, JEOL JSM-6490). The bulk densities were measured by Archimedes method. Complex permeability, permittivity, and dielectric loss tangent were measured by the impedance analyzer (HP4291B) in the frequency range of 1 MHz–1.8 GHz. The saturation magnetization was measured by the vibrating sample magnetometer (MODEL BHV-525).

3. Results and discussion

Fig. 1 shows the XRD patterns of samples with different BIT contents sintered at 900 °C. The parent phases of the BIT and NCZF in adequate proportions (corresponding to the indicated compositions) were found, confirming the successful preparation of two-phase composites. A comparison between the XRD patterns of composites reveals that the number of peaks of ferroelectric phase and intensity of BIT peaks increase with increasing percentage of BIT in the composites.

Fig. 2 shows the effect of BIT content on the microstructure of the samples sintered at 900 °C. The grains of NCZF [Fig. 2(a)], having the size less than 1 μm, are fine and uniform without evident growth. The BIT ceramic [Fig. 2(f)], having many lathlike grains lager than 5 μm, shows relatively clear microstructure. For the composite with x = 10 wt% [Fig. 2(b)], many grains with a size of about 5–15 μm are much larger than those of NCZF, indicating that ferrite grain growth can be effectively promoted with the effect of an appropriate amount of BIT [17]. Furthermore, some relatively larger open pores and small close pores are also can be observed in the sintered body. For the composite with x = 30 wt% [Fig. 2(c)], the size of relatively larger grains decrease to about 5 μm, meanwhile, the size and quantity of open pores decrease obviously. When x = 50 wt% [Fig. 2(d)], the grain microstructures observed in the sample with x = 10 wt% and pure BIT ceramic disappear completely, indicating that a homogeneous composite system is obtained. When x = 90 wt% [Fig. 2(e)], the BIT grain growth has been effectively suppressed by a small amount of ferrite, resulting in no obvious grain boundaries.

Fig. 3 shows the relative density of the composites sintered at 900 °C as a function of BIT content. The density of the composites is in the range of 94.9–96.4% of the theoretical density of the composites. The relatively lower density (94.9%) is obtained in the sample with x = 10 wt% due to existence of larger open pores in their microstructures. Among the composites, the relative density reaches the highest value (96.4%) in the sample with x = 30 wt% and decreases slowly with the continuous increase of BIT content. At a certain sintered temperature, variation of the relatively density is affected by different distributions of two phases in each composite, which results in the forming of different types of microstructures. When the mass ratio of two phases reaches an appropriate value, just like 3:7 (x = 30 wt%), it forms a more compact microstructure with less pores. In addition, other ratios such as 1:9 (x = 10 wt%) and 5:5 (x = 50 wt%), which deviate from the appropriate value, cause to form the relatively poor microstructures which lead to somewhat decrease of the density. The theoretical densities of the composites are calculated using the formula [18]:

$$D_x = \frac{W_1 + W_2}{(W_1/D_1) + (W_2/D_2)} \quad (1)$$

where W_1 and W_2 are the weight percentage of NCZF and BIT with the theoretical densities D_1 and D_2, respectively.

Fig. 4 and Fig. 5 show the frequency dependence of the complex permeability for μ' (the real part) and μ'' (the imaginary part), respectively. The permeability μ', at first, has a significant increase in the value accompanying with the increase in the peak value of permeability μ'', and then, decreases gradually with the increase of BIT content. Here variation of both the saturation magnetization M_s and the permeability μ (at 1 MHz) with BIT content, as shown in Fig. 6, is presented to help explain the change in the real part of the permeability. When BIT content increases from 0 to 90 wt%, M_s decreases from 2.85×10^5 A/m to 1.6×10^4 A/m, and μ increases from 26.4 to 170 at first, and then gradually decreases from 170 to 1.4. For polycrystalline ferrite or ferrite composite, there are two types of magnetizing processes, domain wall motion and spin rotation [19,20], which make contribution to the permeability and can be expressed as:

$$\mu = 1 + \chi_{dw} + \chi_{spin} \quad (2)$$

where χ_{dw} and χ_{spin} denote the magnetic susceptibility of domain wall motion and spin rotation, respectively. Moreover, χ_{dw} and χ_{spin} may also be written as [21]:

$$\chi_{dw} = \frac{3\pi M_s^2 D}{4\gamma} \quad (3)$$

$$\chi_{spin} = \frac{2\pi M_s^2}{K_u} \quad (4)$$

where M_s is the saturation magnetization, D is the grain diameter, γ is the wall energy, and K_u is the total anisotropy. According to the Globus model, the increase in average grain size leads to more domain wall contribution to permeability [22]. Though M_s of the sample with x = 0 is larger than that of the sample with x = 10 wt%, the latter has a much larger grain size than the former. Therefore, more contribution of domain wall motion may leads to evident increase of permeability with BIT content increasing from 0 to 10 wt%. Thereafter, ferrite grain growth in composites has been gradually inhibited by a continuous increase in BIT content. Then, the permeability decreases with the decrease of M_s when BIT content increases beyond 10 wt%. As BIT content increases from 10 wt% to 90 wt%, the peak value of permeability μ'' shifts to higher frequencies (the cut-off frequency increases from 26.2 MHz to 404 MHz), accompanying with

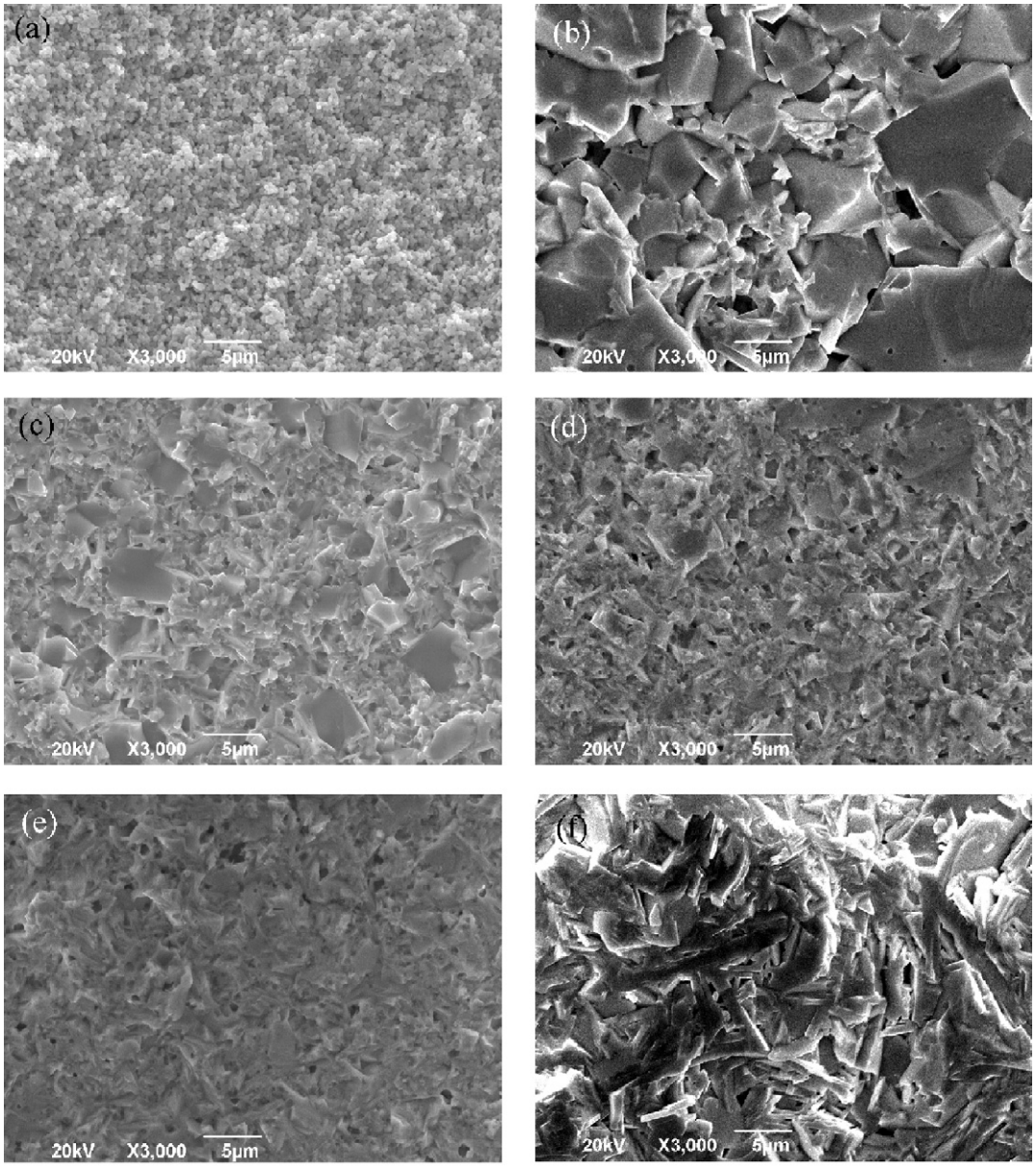

Fig. 2. SEM micrographs of cross sections for (a) $x = 0$ wt%, (b) $x = 10$ wt%, (c) $x = 30$ wt%, (d) $x = 50$ wt%, (e) $x = 90$ wt%, and (f) $x = 100$ wt%.

the decrease of permeability μ', which conforms to the Snoek's law [23].

Fig. 7 and Fig. 8 show the frequency dependence of the complex permittivity for ε' (the real part) and ε'' (the imaginary part), respectively. As BIT content increases from 0 wt% to 90 wt%, the permittivity ε' increases from 8.8 to 100.3 at 1 MHz. Furthermore, ε' of the sample with $x = 90$ wt% has higher value than that of BIT below 650 MHz. For samples with $x = 0$ wt% and 10 wt%, no evident peak occurs in permittivity ε'' below 1.8 GHz. When BIT content increases from 30 wt% to 100 wt%, the peak of permittivity ε'' is evident and shifts from 1.15 GHz to 1.8 GHz. The insert in Fig. 8 shows the variation of dielectric loss tangent (measured at 1 MHz) with BIT content. When BIT content is up to 10 wt%, the loss tangent has a maximum value about 0.47 at first, and then decreases sharply with the increase of BIT content ($\tan\delta < 0.03$ as $x = 70$ wt%).

The relationship between electromagnetic properties and composition of the samples has been modeled using the effective medium theory. For this two-phase medium, we made an attempt to analyze the measured results by the Maxwell-Garnett mixing rule [2,24]:

$$\frac{\psi_{eff} - \psi_e}{\psi_{eff} + 2\psi_e} = \frac{f(\psi_i - \psi_e)}{\psi_i + 2\psi_e} \tag{5}$$

where ψ_{eff} is either the permeability or permittivity for the effective medium, ψ_e for the host medium, and ψ_i for the embedded inclusions with volume fraction f. Here, μ'_{eff} and ε'_{eff} of the samples with different compositions are calculated using appropriate μ' and ε' of BIT and NCZF. When the sintered temperatures of BIT and NCZF are ascertained, μ' and ε' can be measured and different bounds of permeability (or permittivity) can be determined by assuming BIT and NCZF to be matrixes, respectively. Among the samples sintered at 900 °C, it can be observed that μ' (at 1 MHz) of the sample with $x = 10$ wt% is higher than that of NCZF, and similarly ε' (at 1 MHz) of the sample with $x = 90$ wt% is higher than that of BIT. The findings indicate that there is not only a simple mixing process of two phase materials, but also a promotion effect of one phase on the

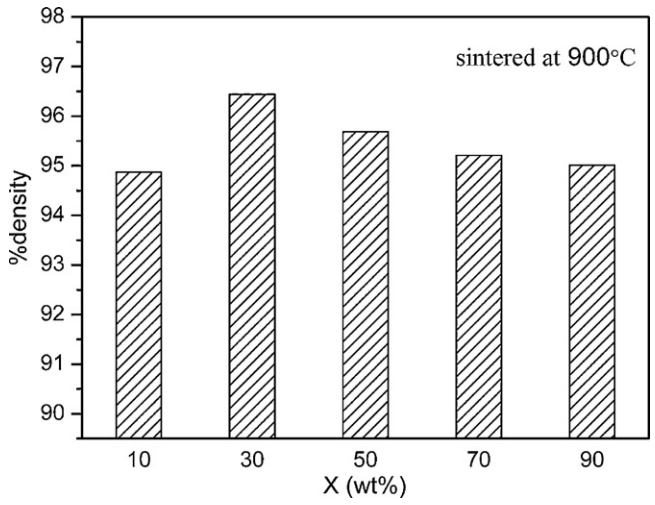

Fig. 3. Variation of the relative density with BIT content for the composites sintered at 900 °C.

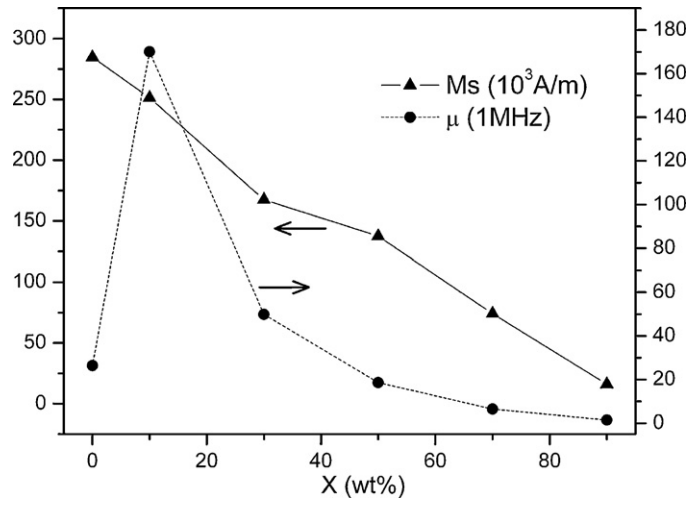

Fig. 6. Variation of the saturation magnetization M_s and the permeability μ (at 1 MHz) with BIT content for the samples sintered at 900 °C.

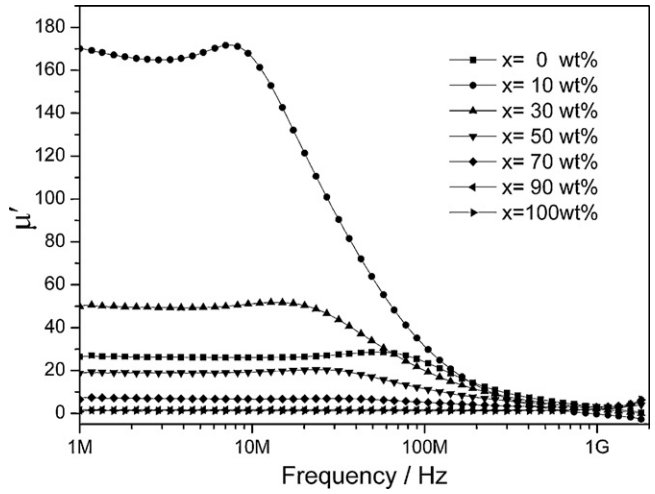

Fig. 4. Variation of the permeability μ' with frequency for the samples sintered at 900 °C.

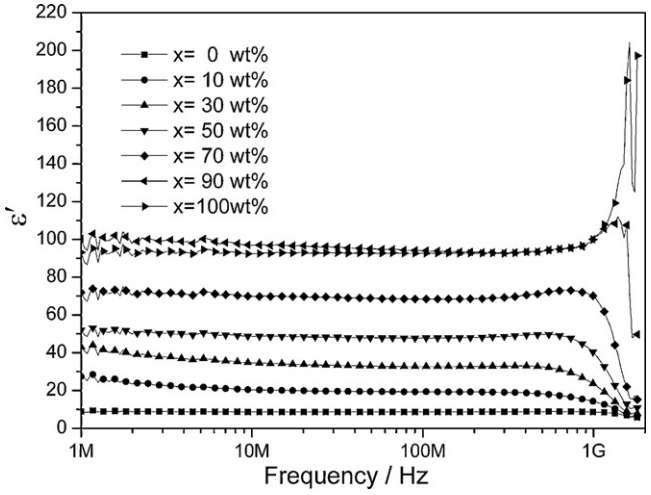

Fig. 7. Variation of the permittivity ε' with frequency for the samples sintered at 900 °C.

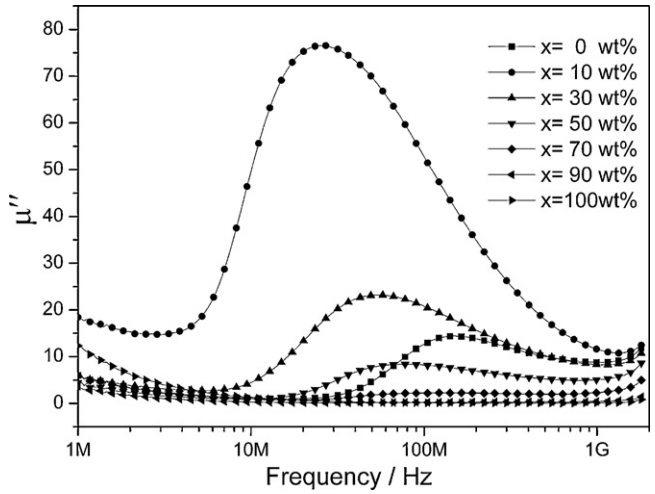

Fig. 5. Variation of the permeability μ'' with frequency for the samples sintered at 900 °C.

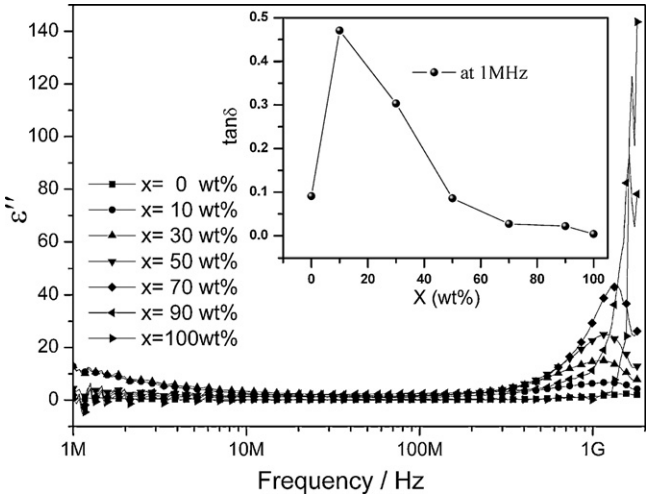

Fig. 8. Variation of the permittivity ε'' with frequency for the samples sintered at 900 °C. The insert shows the variation of dielectric loss tangent (measured at 1 MHz) with BIT content.

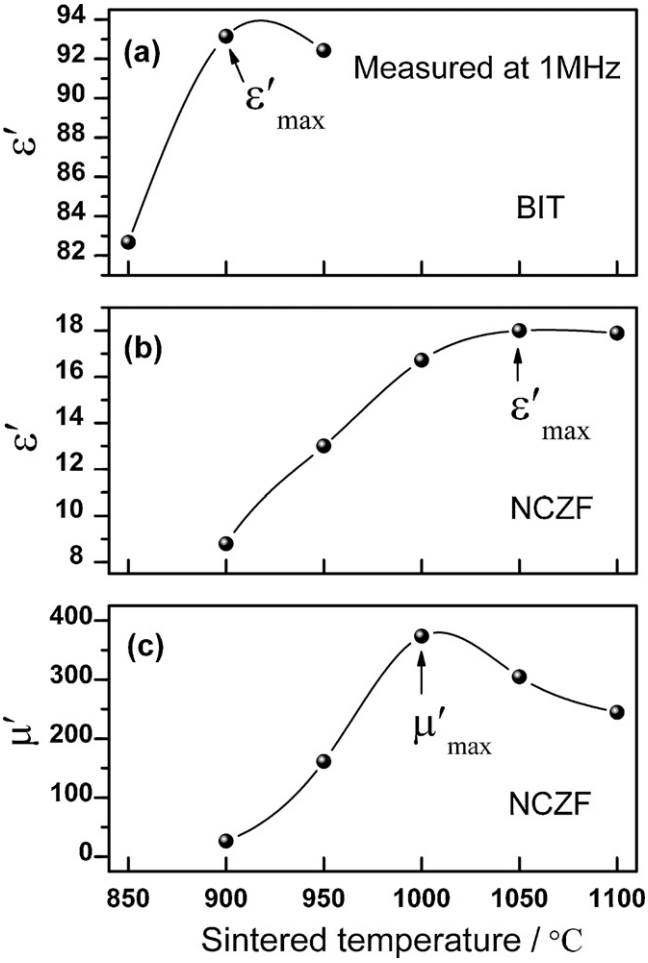

Fig. 9. Variation of ε' and μ' with sintered temperature for BIT and NCZF: (a) $\varepsilon' - T$ for BIT, (b) $\varepsilon' - T$ for NCZF, and (c) $\mu' - T$ for NCZF.

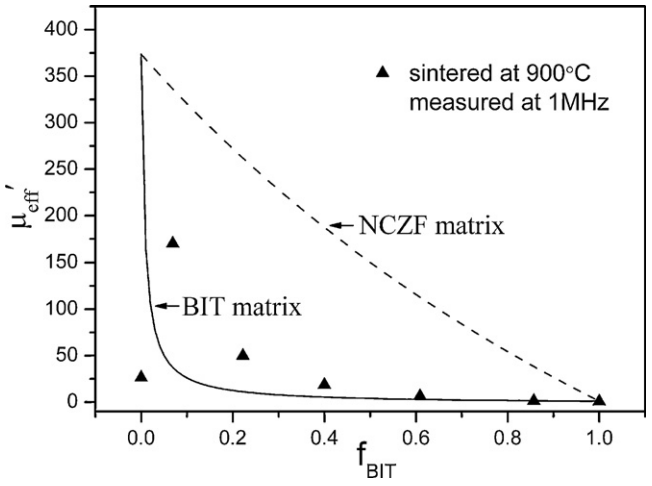

Fig. 10. Measured and Maxwell-Garnett formula calculated μ' versus BIT volume fraction.

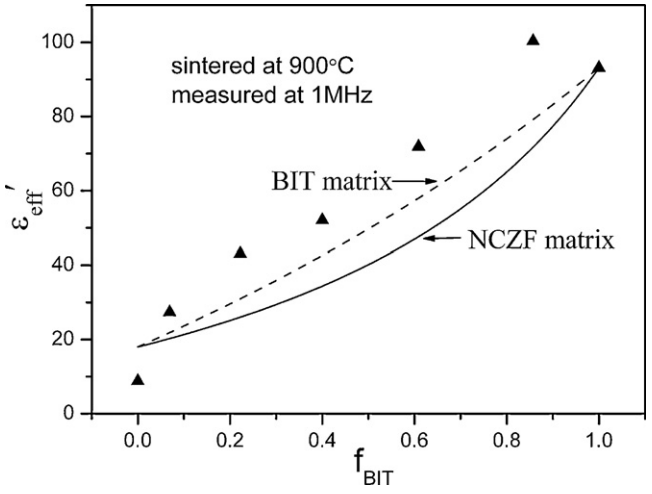

Fig. 11. Measured and Maxwell-Garnett formula calculated ε' versus BIT volume fraction.

performance of the other phase in some samples, just like influence of BIT on ferrite grain growth. Hence, it is necessary to analyze the variation of ε' and μ' with sintered temperature in BIT and NCZF, and ascertain the corresponding maximums for calculating different bounds. The BIT ceramic, as nonmagnetic phase, has the value of μ' set to 1, and furthermore, has ε'_{max} [Fig. 9(a)] corresponding to the sintered temperature 900 °C. Likewise, for the ferrite, ε'_{max} and μ'_{max} occurs at 1050 °C [Fig. 9(b)] and 1000 °C [Fig. 9(c)], respectively.

When the formula (5) is used for predicting the magnetic properties, ψ_e and ψ_i are replaced by μ'_e and μ'_i, and two calculated lines (solid line and dashed line), as shown in Fig. 10, display the variation of μ'_{eff} with BIT volume fraction f_{BIT} assuming BIT and NCZF as matrixes, respectively. For BIT matrix, solid lines are obtained using $\mu'_e = 1$ and $\mu'_i = \mu'_{max}$ of NCZF. Likewise, for NCZF matrix, dashed lines are obtained using $\mu'_e = \mu'_{max}$ of NCZF and $\mu'_i = 1$. It is observed that all measured points are in the area surrounded by two lines except for the point ($f_{BIT} = 0$) corresponding to the ferrite, which has incomplete grain growth at 900 °C. When f_{BIT} is beyond 0.4 (x = 50 wt%), the measured results have a good consistence with the solid line calculated having BIT as matrix. When the formula (5) is used for predicting the dielectric properties, ψ_e and ψ_i are replaced by ε'_e and ε'_i, respectively. Fig. 11 shows the variation of ε'_{eff} with f_{BIT} when BIT or NCZF is regarded as matrix. For BIT matrix, dashed lines are obtained using $\varepsilon'_e = \varepsilon'_{max}$ of BIT and $\varepsilon'_i = \varepsilon'_{max}$ of NCZF. Likewise, for NCZF matrix, solid lines are obtained using $\varepsilon'_e = \varepsilon'_{max}$ of NCZF and $\varepsilon'_i = \varepsilon'_{max}$ of BIT. It can be found that lines obtained with BIT matrix are more close to the measured points in comparison with that obtained with NCZF matrix. The Maxwell Garnett mixing formula is concluded from the model that inclusions in the mixture are spherical and randomly distributed. Considering the shape of ferrite grain (cubic) and BIT grain (lathlike), assuming the former as embedded inclusions is more accord with the model. Hence, the calculation basing on BIT matrix is more approximate to the actual results. In addition, neither of two lines obtained with BIT matrix can completely represent the variation of measured results. The evident enhancement in ε' at the measured point with $f_{BIT} = 0.86$ (x = 90 wt%) cannot be explained accurately by the Maxwell Garnett mixing rule and needs further research.

4. Conclusions

1. The BIT/NCZF ferroelectric–ferromagnetic composites have been prepared by solid-state reaction at 900 °C and can be applied in LTCC technology. The XRD patterns showed that ferrite phase and BIT phase coexist in the composites.
2. Among the composites, the sample with x = 10 wt% has the relatively lower density 94.9% due to existence of larger open pores in their microstructures. The relative density reaches the highest

value (96.4%) in the sample with x = 30 wt% and decreases slowly with the continuous increase of BIT content.

3. As BIT content increases from 0 to 90 wt%, M_s decreases from 2.85×10^5 A/m to 1.6×10^4 A/m, and μ at 1 MHz reaches the maximum 170 with 10 wt% BIT at first, and then gradually decreases from 170 to 1.4. More contribution of the domain wall motion should be responsible for the relatively higher value of permeability in the composite with 10 wt% BIT. The permittivity ε' increases with BIT content increasing from 0 wt% to 90 wt%.
4. The Maxwell Garnett mixing rule has been used for predict magnetic and dielectric properties of the composites with different assumptions. As BIT is regard as matrix, the measured μ' of samples with BIT content beyond 50 wt% have a good consistence with the calculated curve, and the calculated ε' of samples are more approximate to the measured in comparison to that obtained with NCZF matrix.

Acknowledgements

This work is partly supported by the Scientific Research Foundation of CUIT (No. KYTZ201210), the Foundation for Innovative Research Groups of the NSFC (No. 60721001), the National Natural Youth Fund of China (No. 61001025), the Scientific Fund for College (No. ZYGX2011X006), the Fund of Guangdong Province for Research and Industrialization (No. 2010B090400314), and the Outstanding Doctoral Fund of UESTC (No. A01002203901048).

References

[1] T. Yamamoto, M. Chino, R. Tanaka, T. Ueyama, K. Okazaki, Ferroelectrics 95 (1989) 175–178.
[2] J.V. Mantese, A.L. Micheli, D.F. Dungan, R.G. Geyer, J. Baker-Jarvis, J. Grosveror, J. Appl. Phys. 79 (1996) 1655–1660.
[3] X. Qi, J. Zhou, Z. Yue, Z. Gui, L. Li, S. Buddhudu, Adv. Funct. Mater. 14 (2004) 920–926.
[4] J. Huang, P. Du, L. Hong, Y. Dong, M. Hong, Adv. Mater. 19 (2007) 437–440.
[5] H. Zhang, H. Zhong, B. Liu, Y. Jing, Y. Liu, IEEE Trans. Magn. 41 (2005) 3454–3456.
[6] W. Ling, H. Zhang, Y. Li, Y. Xie, Y. He, L. Peng, F. Bai, J. Appl. Phys. 105 (2009) 07D911.
[7] W. Ling, H. Zhang, Y. Li, D. Chen, Q. Wen, J. Shen, J. Appl. Phys. 107 (2010) 09D911.
[8] S.S. Kalarickal, D. Ménard, J. Das, C.E. Patton, X. Zhang, L.C. Sengupta, S. Sengupta, J. Appl. Phys. 100 (2006) 084905.
[9] X. Qi, J. Zhou, B. Li, Y. Zhang, Z. Yue, Z. Gui, L. Li, J. Am. Ceram. Soc. 87 (2004) 1848–1852.
[10] J. Shen, Y. Bai, J. Zhou, L. Li, J. Am. Ceram. Soc. 88 (2005) 3440–3443.
[11] R.T. Hsu, T.M. Peng, J.H. Jean, Jpn. J. Appl. Phys. 45 (2006) 5841–5846.
[12] P.V. Petrov, A.S. Tatarenko, S. Pandey, G. Srinivasan, J.V. Mantese, R. Azadegan, Electron. Lett. 44 (2008) 506–507.
[13] Y. Imanaka, Multilayered Low Temperature Cofired Ceramics (LTCC) Technology, Springer, New York, 2005.
[14] S. Thomas, M.T. Sebastian, Mater. Res. Bull. 43 (2008) 843–851.
[15] A. Fouskova, L.E. Cross, J. Appl. Phys. 41 (1970) 2834–2838.
[16] L.B. Kong, J. Ma, W. Zhu, O.K. Tan, Mater. Lett. 51 (2001) 108–114.
[17] W. Ling, H. Zhang, Y. He, Y. Wu, K. Yang, Y. Li, S. Li, J. Magn. Magn. Mater. 322 (2010) 819–823.
[18] T. Takada, S.F. Wang, S. Yoshikawa, S.J. Jang, R.E. Newnham, J. Am. Ceram. Soc. 77 (1994) 1909–1916.
[19] G.T. Rado, Rev. Mod. Phys. 25 (1953) 81–89.
[20] T. Nakamura, T. Tsutaoka, K. Hatakeyama, J. Magn. Magn. Mater. 138 (1994) 319–328.
[21] P.I. Slick, Ferrites for non-microwave applications, in: E.P. Wohlfarth (Ed.), Ferromagnetic Materials, Elsevier Science B.V., Amsterdam, 1986, pp. 208–209.
[22] A. Globus, M. Guyot, IEEE Trans. Magn. 6 (2005) 614–617.
[23] J.L. Snoek, Physica 14 (1948) 207–217.
[24] A. Sihvola, Electromagnetic Mixing Formulas and Applications, The institution of Electrical Engineers, London, 1999.